Journal of ELECTRONIC MATERIALS
https://doi.org/10.1007/s11664-020-08495-y

The Effect of Deposition Time on the Properties of Cu_2O Nanocubes Using an Electrochemical Deposition Method

SHIVAN JAWHAR TAHER,[1] AZEEZ ABDULLAH BARZINJY,[2,3,6] and SAMIR MUSTAFA HAMAD[4,5]

1.—Pharmacy Department, Medical Institute, Erbil Poly Technique University-Erbil, Erbil, Iraq. 2.—Department of Physics, College of Education, Salahaddin University-Erbil, Erbil, Iraq. 3.—Department of Physics, Education, Faculty of Education, Tishk International University, Erbil, Iraq. 4.—Scientific Research Centre, Soran University, Soran 44008, Erbil, Iraq. 5.—Computer Department, Cihan University-Erbil, Erbil, Iraq. 6.—e-mail: azeez.azeez@su.edu.krd

In this investigation, the impact of electrodeposition time on the photoelectrochemical characteristics of a cuprous oxide (Cu_2O) nanocube semiconductor photoelectrode is investigated. The Cu_2O nanocube photoelectrode was synthesized electrochemically, utilizing underpotential deposition (UPD). Numerous techniques, including x-ray diffraction (XRD), scanning electron microscopy (SEM), energy-dispersive x-ray spectroscopy (EDX), ultraviolet–visible (UV–Vis) spectroscopy, linear sweep voltammetry (LSV) and chronoamperometry (CA), were utilized for characterization of the Cu_2O nanocube photoelectrode. A highly crystalline structure of Cu_2O nanocubes deposited on an indium tin oxide (ITO) substrate can be seen in the XRD results. SEM images revealed a cubic-shaped structure of Cu_2O. However, EDX analysis and the optical bandgap confirmed the presence of uniform single-phase Cu_2O nanocubes. Astonishingly, the Cu_2O nanocube photoelectrode electrodeposited for 15 min possesses the highest photocurrent among all investigated films. Also, the Cu_2O nanocubes displayed stable photocathodic performance as a result of the *p*-type nature. Moreover, the Cu_2O nanocube photoelectrode is suggested to be a good candidate for progressive photoelectrochemical detection. Furthermore, it can be utilized for the expanded field of photoelectrochemical water splitting in addition to other solar photovoltaic devices.

Key words: Cuprous oxide, electrochemical deposition, deposition time, underpotential deposition, photo-electrochemistry

INTRODUCTION

Electrochemistry deals with chemical changes related to charge splitting, typically in a liquid medium.[1] The splitting of charge is frequently associated with charge transmission, which might happen evenly in solution among diverse chemical classes, or heterogeneously on electrode surfaces.[2] Accordingly, it can be seen that its requirements are exceedingly widespread among the investigators. Above the electrode surfaces, the oxidation and reduction half replies are divided in space, typically happening at diverse electrodes submerged in solution.[3] The electrodes are connected through conducting routes together in solution, using ionic transportation. Once the totality of the Gibbs energy altered correspondingly at the electrodes is negative, the electrical energy released can be joined. However, if the Gibbs energy is positive, outward electrical energy can be provided to overcome the positive Gibbs energy change.[4] Therefore, if the cell shape licenses, the products of the two

(Received June 11, 2020; accepted September 16, 2020)

Published online: 12 October 2020

electrode responses can be disconnected, as happens in manufacturing electrolytic responses. On the other hand, photoelectrochemistry, as an active field of investigation, is a branch of chemistry that deals with the interaction of light with electrochemical systems.[5]

It can be stated that cuprous oxide (Cu_2O) is a *p*-type semiconductor with a direct bandgap of 2.0 eV.[6] It can absorb solar energy to the extent of 300–620 nm, which covers about half of the photons of the solar spectrum.[7] Cuprous oxide is classified as a candidate photocathode for photoelectrochemical cells. Since the upper part of the conduction band of Cu_2O is nearly −1.35 V, it is sufficiently more negative than the reduction potential of water, −0.61 V.[8] Accordingly, the generation of H_2 fuel from water and visible light necessitates photoelectrodes, such as Cu_2O, that are inexpensive, stable and highly reactive.[9] Photoelectrochemical cells are considered as solar cells that are capable of changing light sources into electrical energy.[10] Every single cell comprises a photocathode and a metal anode that is immersed in a semiconducting electrolyte. The foundation of solar cell systems in semiconductor technology has recently become very significant for energy production. Also, the main properties of semiconductor material make them appropriate as vital components in electronic circuits.[11] A photoelectrochemical procedure takes place through the following steps. Firstly, an electronic charge is formed on the surface of a photocathode sensitive to the sun's light, producing electron–hole pairs. Secondly, electrons and protons in the photocathode are reduced to hydrogen molecules. Lastly, conduction of the photocathodically anodic holes occurs through an electrolytic and electrical connection.[12]

It can be noted that Cu_2O thin films can be produced through numerous methods. Amongst these, the electrodeposition method has garnered increasing attention in recent years for producing Cu_2O thin films.[13] This method has two key benefits, specifically its ease of use and the low growth temperature, resulting in lower-cost procedures and a great number of manufacturing requests. Likewise, electrodeposition permits controlling of the stoichiometry, thickness and microstructure of the films by adapting the deposition factors.[14] Till now there have been some researches exploring the impact of pH on the preferred alignment of the Cu_2O crystallites that form the film, but few mechanical details were deliberated.[15] On the other hand, the energy band alignment at the heterointerface between Cu_2O and other oxide materials, such as zinc oxide (ZnO), was investigated using photoelectron spectroscopy with stepwise deposition of oxide materials onto Cu_2O and vice versa. It can therefore be ascribed to a pinning of the Fermi level in oxide materials and Cu_2O, which can be traced back to oxygen vacancies in oxide materials and to metallic precipitates in Cu_2O.[16]

In this investigation, the electrodeposition process was performed to synthesize Cu_2O films with varied preferred crystal arrangements. The significance of the deposition time on the morphology, size and the structural characteristics of the Cu_2O films was studied using underpotential deposition (UPD). The UPD potential for copper was determined by cyclic voltammetry (CV) measurements. The photoelectrochemical characteristics of the grown Cu_2O films were studied in the dark and under light radiance. X-ray diffraction (XRD) and scanning electron microscopy (SEM) measurements were performed to check the stability and the structure of the Cu_2O films. Finally, the electrodeposition of Cu_2O nanostructures with numerous dimensions on the indium tin oxide (ITO)-coated electrode surface was also investigated intensively.

MATERIALS AND METHODS

Copper sulfate pentahydrate ($CuSO_4{\cdot}5H_2O$), sodium sulfate (Na_2SO_4), lactic acid ($C_3H_6O_3$), sodium hydroxide (NaOH), sulfuric acid (H_2SO_4), ethanol (C_2H_6O) and acetone (C_3H_6O) were used as received from Sigma-Aldrich Company.

An aqueous basic solution containing 0.02 M $CuSO_4$, 0.2 M Na_2SO_4 and 0.3 M lactic acid solution, such as an environment prepared by semiconducting materials were utilized by the electrochemical method. The pH of the solutions was adjusted to 9 with NaOH and H_2SO_4 and monitored with a Denver Instruments SI-234 pH meter. An Orion 3-Star ultrasonic mixer was used for mixing the chemicals homogeneously in the experiments. An Apple S 60 H deionized water device was used to provide distilled water for the dissolution process. A Human Power 1 electrochemical analyzer was used to monitor the linear sweep voltammograms (LSV). A Princeton Applied Research PAR 283 potentiostat with a three-electrode system was used for thin-film preparation by an electrochemical method. A CH Instruments CHI 6096E XRD system was used to verify the phase and orientation of the deposited films. A JEOL JSM-6510 SEM was used to characterize the morphology of the Cu_2O films. A Rigaku Ultima IV energy-dispersive x-ray (EDX) used for elemental analysis process. A JEOL JSM-6510 UV–Vis–NIR spectrophotometer was utilized for calculating the bandgaps of Cu_2O films from the optical absorbance in a wavelength range of 300–800 nm. A Shimadzu UV-3600 spectrophotometer and Solar Light 16S-002 solar simulator were used for photoelectrode analysis.

The electrochemical deposition of Cu_2O films was carried out using a PAR 283 potentiostat in a three-electrode configuration (Fig. 1). ITO served as the working electrode (substrate), and a platinum sheet served as the counter electrode. For the deposition in pH 9 solutions, the reference electrode was a Ag/AgCl electrode with a bridging saturated potassium

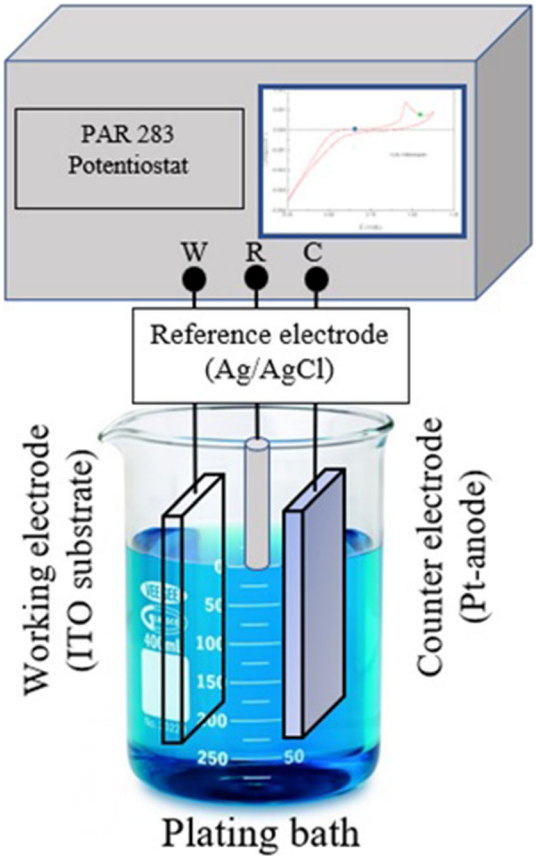

Fig. 1. Schematic representation of electrochemical deposition of Cu_2O film on ITO substrate.

chloride (KCl) solution, and all potentials are referred to the Ag/AgCl electrode unless stated otherwise. All the plating solutions were kept at room temperature during the electrodeposition process. Electrochemical reactions were performed in cells with three electrodes. The reference electrode, working (cathode) electrodes and counter (anode) electrodes were immersed in an electrolyte solution (plating bath). Thus, the oxidation/reduction (redox) reactions took place. The reduction reactions took place on the cathode electrode, while the oxidation reactions took place on the anode electrode. In addition, the three electrodes were placed in separate compartments in the PAR 283 potentiostat. The electrodeposition was operated at 0.1 V for different times with a PAR 283 potentiostat.

RESULTS AND DISCUSSION

Electrochemical Studies

This study originally focused on homogeneous Cu_2O photoelectrode synthesis as a function of deposition time using the UPD-based electrochemical technique. In principle, UPD occurs when the electrochemical deposition of a metal onto a substrate at potentials is more positive than the Nernst potential.[17] It is usually constrained to the formation of one atomic layer of the deposited metal.

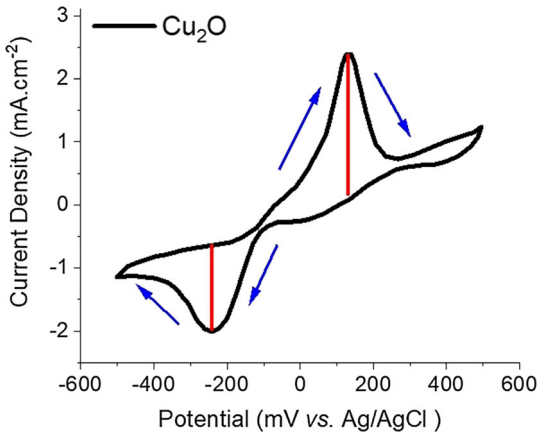

Fig. 2. Cyclic voltammogram of Cu_2O on ITO electrode recorded in 0.02 M $CuSO_4$ solution at a potential sweep rate of 20 mV/s.

Therefore, to deposit one atom at a time, very small amounts of dissolved copper and oxygen species are needed in the solution phase for UPD. The UPD potential for copper was determined by cyclic voltammetric measurements.[18] To determine a deposition potential of copper (I) oxide from the solution, the cyclic voltammetric measurements of copper were also recorded at the UPD region in the aqueous medium (Fig. 2).

The cyclic voltammetric technique was utilized in the first step to prepare copper oxide semiconductors, and the voltammogram was taken in the range from −500 mV to 500 mV. This technique was utilized to determine the electrodeposition potential for the preparation of semiconductors, and to provide methodical nucleation. The second step involved the utilization of the controlled potential electrolysis technique at the determined potential; electrodeposition was realized throughout 15 min. The UPD region, where surface-limited electrochemical reactions were realized, was preferred as the electrodeposition potential region over the bulk deposition or overpotential deposition region. In similar investigation, Arifin et al. carried out cyclic voltammetry measurement to determine the ideal potential range for fabrication of *p*-type Cu_2O on *n*-type Cu_2O/FTO substrate.[19] They found that these potential values were variable with the selected pH values of 12.0 and 12.5 to fabricate the *p*-type Cu_2O thin film.

The results showed that the bulk Cu deposition does not occur until −200 mV. If the potential of the working electrode is kept constant at a more positive potential than −200 mV, copper and oxygen are supposed to deposit underpotentially at the ITO-coated electrode surface. The electrodeposited Cu and O react to form a Cu_2O semiconductor on the ITO-coated surface. Bijani et al. indicated that the amount of electrodeposited Cu_2O depends on the deposition time.[20] Thus, electrodeposition of Cu_2O nanostructures with various dimensions on the

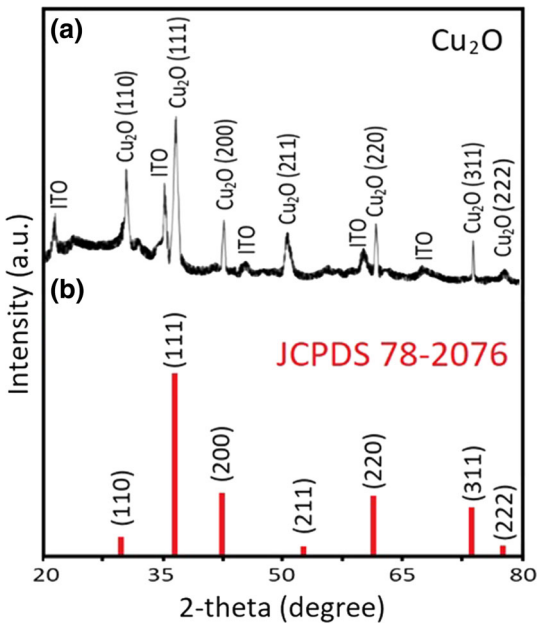

Fig. 3. (a) The XRD of Cu_2O photoelectrodes electrodeposited for 15 min on ITO substrate in comparison with (b) the JCPDS standard.

ITO-coated electrode surface could be achieved by this method using different deposition times.

XRD Studies

Figure 3 represents the XRD of Cu_2O nanocube photoelectrodes electrodeposited for 15 min. The XRD of copper (I) oxide consists of a strong diffraction peak at 36.6° arising from (1 1 1) reflections from Cu_2O. The weaker diffractions at 42.5°, 61.7° and 73.9° correspond to (2 0 0), (2 2 0) and (3 1 1) reflections of Cu_2O, respectively. The other peaks belong to ITO-coated glass which served as the working electrode in this investigation. The XRD analyses showed that all Cu_2O thin films were in a polycrystalline cubic phase and similar to the standard data of the Joint Committee on Powder Diffraction Standards (JCPDS 78-2076), with preferential orientation in (111) plane. The XRD patterns collected confirmed that all the nanocube samples were indeed Cu_2O, and no other phases of copper oxide were present. The other XRD of Cu_2O at different deposition times were similar to Fig. 3. This indicates that the crystal structures of Cu_2O films were not affected by the change of deposition times. In a comparable investigation, Hossain et al. indicated that the electrodeposition time enhanced the crystallinity of Cu_2O thin film.[21] The only distinct point one can observe from other XRD images is as the deposition time increased, the intensity of Cu_2O diffractions increased. The XRD results in this investigation are a good indicator that Cu_2O nanocubes possess very high crystallinity. Similar results have been obtained by Ma et al.[7]

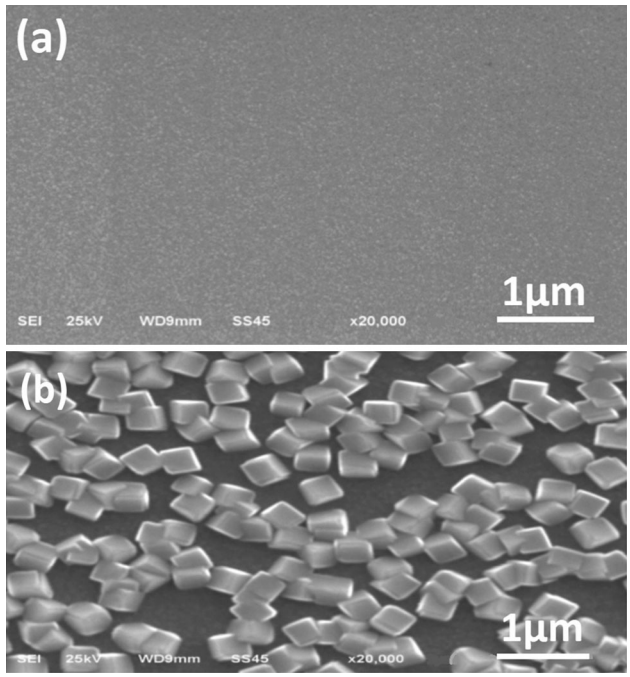

Fig. 4. SEM images of the (a) ITO-coated glass working electrode and (b) Cu_2O photoelectrodes electrodeposited onto the ITO-coated glass surface.

SEM and EDX Analysis

Figure 4a shows the SEM image of the ITO-coated glass surface, which was utilized as a working electrode in this study, while Fig. 4b shows the SEM image for the Cu_2O nanocube semiconductor electrodeposited on the ITO-coated glass for 15 min. The reason behind highlighting this deposition time among all cases is due to the fact that the thin film within 15 min deposition exhibited the highest photocurrent. Evenly distributed Cu_2O nanocubes, of approximately the same size, 200 nm, are observed on the surface of the ITO-coated electrode. Most of the Cu_2O semiconductor nanocubes possess a uniform shape. Recently, Yilmaz et al. stated that the film thickness and crystallite grain size affect the photoelectrochemical activity and stability of Cu_2O film that can be utilized for solar cell applications.[22] The average size of Cu_2O semiconductor nanocubes observed for 15 min were about 200 nm in diameter. The morphology of the Cu_2O grown by electrochemical deposition is similar to the results with an average nanocube size of 200 nm reported in the literature.[23]

It can be observed from this investigation that as the electrodeposition time is increased, the diameters of the Cu_2O nanocubes increase (Fig. 5). The resulting Cu_2O nanocubes in these samples have diameters of approximately 120 nm, 200 nm, 300 nm and 500 nm for 5 min, 15 min, 30 min and 60 min, respectively. Interestingly, these Cu_2O nanocubes, in all conditions, possess high

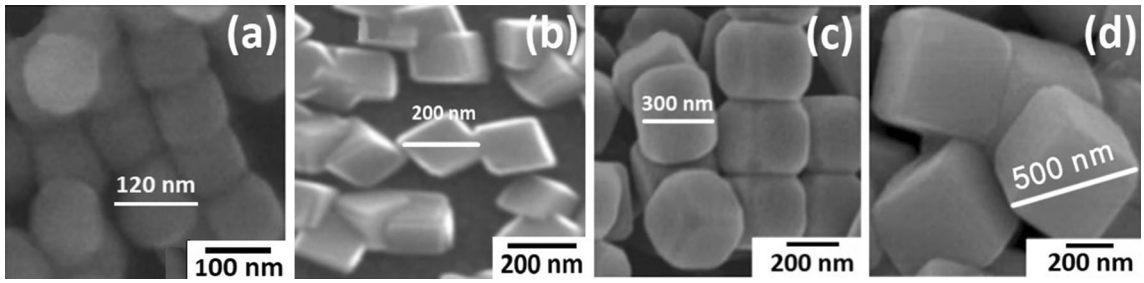

Fig. 5. SEM images of Cu_2O photoelectrodes electrodeposited onto the ITO-coated glass surface for (a) 5 min (b) 15 min (c) 30 min and (d) 60 min.

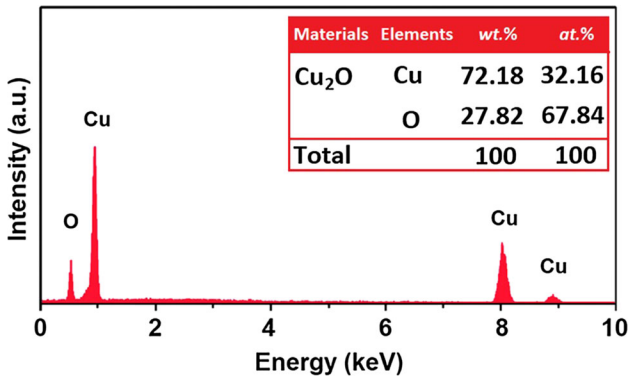

Fig. 6. EDX analysis of Cu_2O photoelectrodes electrodeposited onto the ITO-coated glass surface.

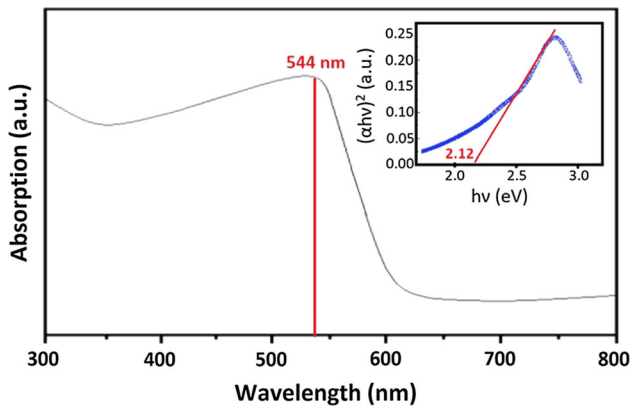

Fig. 7. UV–Vis spectrum of Cu_2O semiconductor photoelectrodes electrodeposited for 15 min on the ITO substrate. Inset: Tauc plot of the same UV–Vis spectrum.

uniformity in size and shape. This is perhaps due to the fact that Cu_2O has a cubic crystal structure, i.e. a body-centered cubic packing of oxygen atoms with copper atoms occupying one-half of the tetrahedral sites. Wang et al. stated that the conductive nature of the Cu_2O-based semiconductor is tunable, permitting the construction of *n*-type and *p*-type, in addition to *p*–*n* junction photoelectrodes.[24]

The elemental composition of the Cu_2O nanocube semiconductor photoelectrodes was determined by EDX analysis (Fig. 6). The lack of appearance of any peaks other than Cu and O is a good indicator that the Cu_2O is homogeneous in composition and formed from Cu–O. Also, EDX analyses from different regions gave the same outcomes. For the copper (I) oxide semiconductors, the quantitative atomic ratios of Cu/O were 32.16:67.84, which is close to 1:2 stoichiometry. Similar outcomes have been obtained by Lenglet et al.[25]

UV–Vis Absorbance and Bandgap Studies

The UV–Vis absorbance spectrum of Cu_2O nanocube semiconductor photoelectrodes electrodeposited for 15 min on the ITO substrate is shown in Fig. 7. It can be seen from Fig. 7 that Cu_2O possesses only one absorption band in the UV–Vis region. The absorption peak measured for the photoelectrodes was 544 nm, which corresponds to the exciton formation in the nanocrystalline Cu_2O.[26] The other absorbance spectrums of Cu_2O semiconductor photoelectrodes at different deposition times were similar to Fig. 7. In a similar study, Li et al.[27] described similar absorption peaks positioned at 539 nm. Also, Sekhar et al.[28] detected a comparable peak of Cu_2O at 547 nm.

For all the semiconductors, the widely used method of plotting $(\alpha h\nu)^2$ versus the energy $h\nu$ was adopted to determine the bandgap of the materials. The E_g can thus be estimated from a plot of $(\alpha h\nu)^2$ versus the photon energy $h\nu$ (Fig. 7 inset). The bandgap of Cu_2O semiconductors electrodeposited onto ITO-coated glass was found to be E_g = 2.12 eV. Between the fine bandgap semiconductor photocatalysts, the cuprous oxide with a direct bandgap of 2.17 eV is very promising due to its exclusive characteristics, for example, *p*-type character, relatively negative conduction band location, low cost, profusion and safety.[29] Recently, there has been increasing attention to the synthetic, morphological and catalytic characteristics of Cu_2O.[30]

Linear Sweep Voltammogram Studies

Figure 8 represents linear sweep voltammograms of Cu_2O nanocube semiconductor photoelectrodes electrodeposited in dark and light as a function of deposition time in 0.1 M Na_2SO_4. Figure 8 also shows the effect of electrochemical deposition time

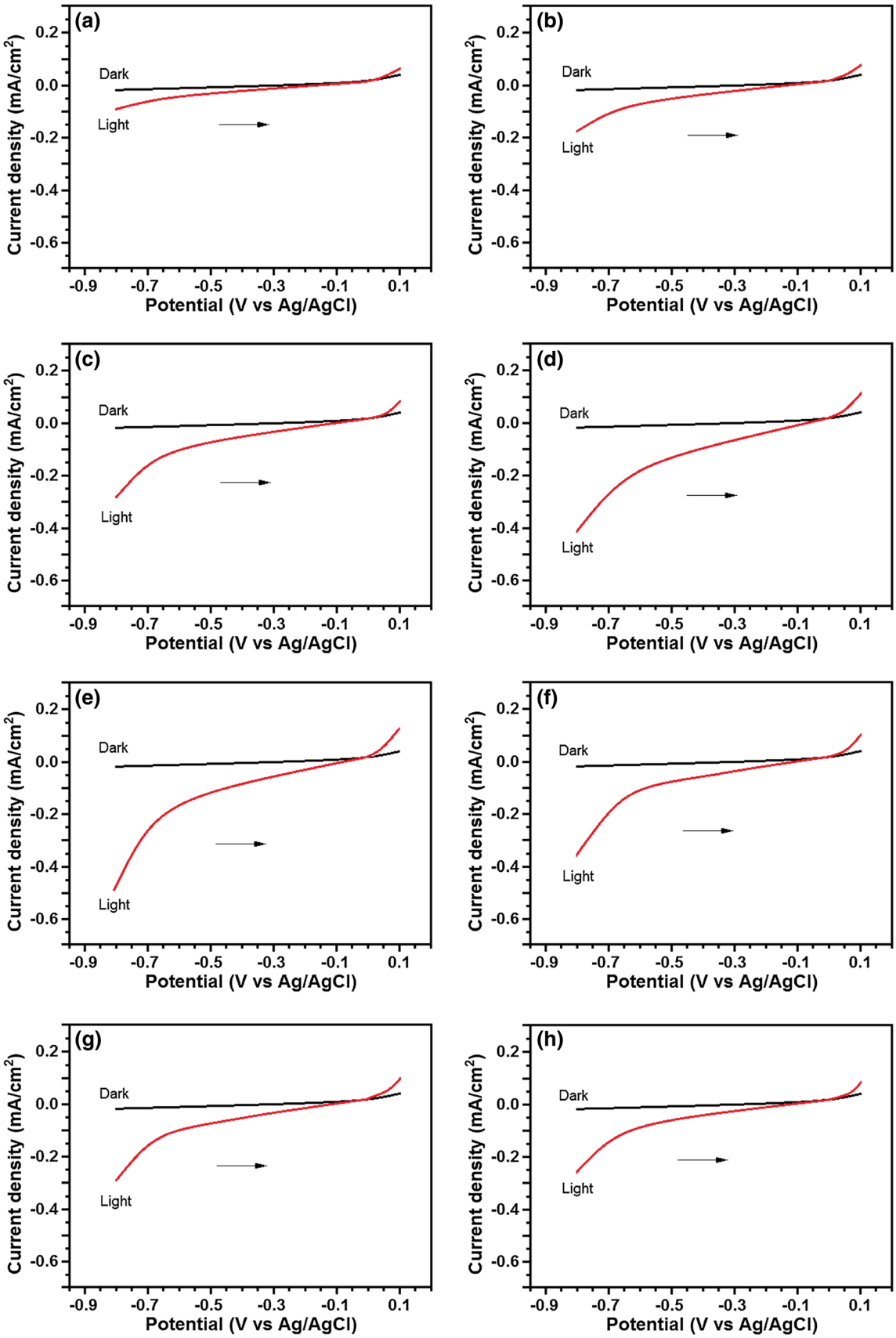

Fig. 8. Linear sweep voltammograms of Cu_2O semiconductor photoelectrodes electrodeposited for (a) 1 min, (b) 3 min, (c) 5 min, (d) 10 min, (e) 15 min, (f) 30 min, (g) 60 min, (h) 120 min and (i) 180 min in 0.1 M Na_2SO_4.

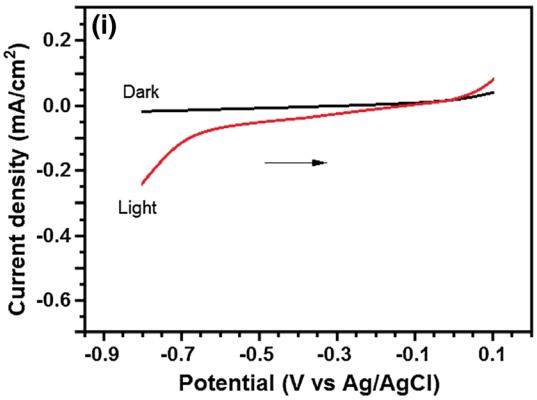

Fig. 8. continued

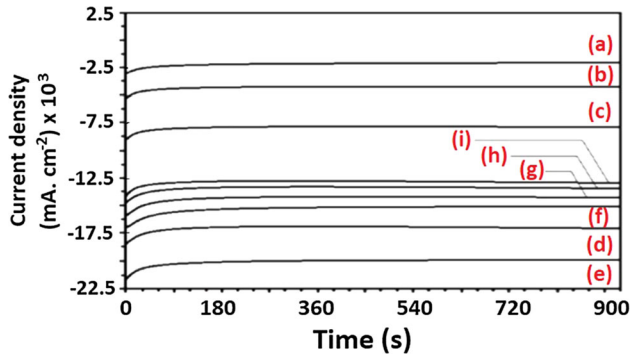

Fig. 9. Current density of copper (I) oxide photoelectrodes electrodeposited for (a) 1, (b) 3, (c) 5, (d) 10, (e) 15, (f) 30, (g) 60, (h) 120 and (i) 180 min under light illumination in 0.1 M Na_2SO_4.

on the light and dark current of Cu_2O semiconductor photoelectrodes. This linear sweep voltammogram exhibited a photocathodic behavior due to the *p*-type nature of the Cu_2O semiconductors in a voltage range of 0.2 V to −0.8 V. Figure 8a represents linear sweep voltammograms of Cu_2O semiconductor photoelectrodes electrodeposited in dark and light for 1 min in 0.1 M Na_2SO_4. In a similar study, Tang et al.[31] showed the electrochemical deposition of nanocrystalline Cu_2O thin films on TiO_2 films coated on transparent conducting optical glass substrates by cathodic reduction of cupric acetate.

Figure 8b shows linear sweep voltammograms of Cu_2O photoelectrodes electrodeposited for 3 min. It can be noticed that the mismatching between the starting points begin to diverge between dark and light and exhibited photocathodic behavior. The photocurrent was increased with longer deposition time. This mismatching became broader at 5 min (Fig. 8c) and 10 min (Fig. 8d) until it reached the highest point at 15 min (Fig. 8e). Surprisingly, after 15 min deposition (Fig. 8e), this trend reversed exactly like the starting deposition time. This is again a good indicator showing that the thin film within 15-min deposition possesses the highest photocurrent of all investigated semiconductor films.

It can be seen from Fig. 8 that 30 min deposition (Fig. 8f) produced a similar trend as 10 min deposition (Fig. 8d), while 60 min deposition (Fig. 8g) resulted in a similar trend as 5 min deposition (Fig. 8c), and 120 min deposition (Fig. 8h) resulted in a similar trend as 3 min deposition (Fig. 8b). Lastly, 180 min deposition (Fig. 8i) was quite close to the case with 1 min deposition (Fig. 8a). This selective analysis indicates the superiority of 15 min deposition among all investigated semiconductor films. It is also worth noting that, beyond 120 min, the photocurrent of Cu_2O semiconductor photoelectrodes remained almost constant. This may be due to the increased bending of Cu_2O semiconductor photoelectrodes for higher deposition times, which may reduce the effective area for surface reactions, leading to lower photocurrent. All the linear sweep voltammograms showed a photocathodic behavior due to the *p*-type nature of the Cu_2O semiconductors. Shyamal et al.[32] demonstrated the preparation of *p*-type Cu_2O thin films using a cathodic electrodeposition method. They also showed that the Cu_2O semiconductor photoelectrodes experience higher ohmic resistance at the electrode solution interface due to a decreased electronic conductivity; better electrical connectivity of a Cu_2O semiconductor can be obtained with metallic Cu and Al substrate as compared with that of ITO-coated glass.[33]

It can be observed that the linear sweep voltammetry of the Cu_2O nanocube semiconductor photoelectrodes under light with a bias more negative than that of the flat-band potential displayed increased photocurrent. This is attributed to the direct bandgap nature of Cu_2O with better charge carrier mobility and carrier lifetime. In addition, it is obvious from the linear sweep voltammograms that the photocurrent increases at a potential which is more negative than the flat-band potential of the corresponding metal oxide. It is also expected that at flat-band potential, there is no net charge transfer and the net current is zero. Nevertheless, the linear sweep voltammogram shows a small current at the flat-band potential for dark and light conditions, which is attributed to the surface states. With Cu_2O being a *p*-type and ITO an *n*-type semiconductor, the nature of the ITO-Cu_2O interface was checked by recording the I–V behavior under dark conditions at the same potential range. The I–V behavior is found to be purely ohmic in nature, ruling out its interference in the water-splitting experiment by acting as a *p*–*n* junction.

Figure 9 illustrates the current density under sunlight for the corresponding copper (I) oxide semiconductor photoelectrodes. Herein, the effect of Cu_2O electrodeposition time on the photocurrent of photoactive films is investigated.

It can be seen from Fig. 9 that as the electrochemical deposition time increased, the current density of Cu_2O semiconductor photoelectrodes increased. The Cu_2O semiconductor photoelectrodes

electrodeposited for 15 min (Fig. 9e) exhibit the highest current density among all the investigated semiconductor films. This is, again, due to the fact that the thin film within 15 min deposition possesses the highest photocurrent of all investigated semiconductor films. In general, as the electrochemical deposition time increased, the current density of Cu_2O semiconductor photoelectrodes decreased. After 120 min (Fig. 9i), the current density of Cu_2O semiconductor photoelectrodes remained almost constant. Also, Cu_2O photoelectrodes exhibit good stability and switching behavior for different Cu_2O electrodeposition times. Qadir et al.[33] stated that a combination of ZnO and Cu_2O semiconductors is remarkable for efficient photovoltaic cells and enhanced photoelectrochemical performance. This can be expected since they form high electronic energy band alignment together and have a controllable electronic structure at the interface.

CONCLUSIONS

In this study, *p*-type direct-bandgap Cu_2O nanocubes were synthesized by an electrochemical process at pH 9 under ambient conditions. This study mainly focused on the synthesis of homogeneous Cu_2O photoelectrodes with various deposition times using a UPD-based electrochemical technique. The UPD study for Cu_2O was determined by cyclic voltammetric measurements. This electrodeposited Cu and O reacted to form the Cu_2O semiconductor on an ITO-coated surface. The amount of electrodeposited Cu_2O was dependent on the deposition time.

The XRD analyses showed that the Cu_2O nanocubes thin films were of a polycrystalline cubic phase with preferential orientation in (1 1 1) planes. SEM study showed evenly distributed Cu_2O nanocubes of approximately the same size on the surface of the ITO-coated electrode. Most Cu_2O nanocubes had a uniform shape, and as the electrodeposition time increased, the diameter of the Cu_2O nanocubes also increased. The EDX analyses indicated that the Cu_2O was homogeneous in composition and was formed from Cu–O. The quantitative atomic ratios of Cu/O were close to 1:2 stoichiometry. The Cu_2O semiconductor photoelectrodes electrodeposited for 15 min exhibited the highest photocurrent and current density among all of the investigated semiconductor films. After 120 min, the photocurrent and the current density of Cu_2O semiconductor photoelectrodes remained almost constant. Linear sweep voltammetry of Cu_2O semiconductor photoelectrodes under light with a bias more negative than that of flat-band potential displayed an increase in the photocurrent. This was attributed to the direct-bandgap nature of Cu_2O with better charge carrier mobility and carrier lifetime. Cu_2O photoelectrodes display good stability and can be utilized in photoelectrochemical water splitting and other solar photovoltaic applications.

ACKNOWLEDGMENTS

The authors would like to thank Soran research center for providing all the facilities to perform the research work. In addition, the authors thank Dr. Mukhtar Ahmed at SISAF, Ulster University, UK, for his valuable assistance throughout this investigation. Finally, sincere thanks go to Dr. David M.W. Waswa at Tishk International University for his diligent proofreading of this manuscript.

CONFLICT OF INTEREST

The authors declare that they have no conflict of interest.

REFERENCES

1. K. Oldham and J. Myland, *Fundamentals of Electrochemical Science: Chapter 3: Electrochemical Cells* (Amsterdam: Elsevier, 2012), pp. 63–106.
2. A. Jafari, K. Tahani, D. Dastan, S. Asgary, Z. Shi, X. Yin, W. Zhou, H. Garmestani, and Ș. Tălu, *Surf. Interfaces* 18, 100463 (2020).
3. Q. Ding, S. Chen, D. Chen, J. Liang, and C. Liu, *Surf. Interfaces* 4, 35 (2016).
4. E. Mariam Thomas, S. Ghimire, R. Kohara, A. Nair Anil, K. Yuyama, Y. Takano, K. George Thomas, and V. Biju, *ACS Nano* 12, 9060 (2018).
5. T. Jiang, T. Xie, W. Yang, L. Chen, H. Fan, and D. Wang, *J. Phys. Chem. C* 117, 4619 (2013).
6. H. Nagai, T. Suzuki, H. Hara, C. Mochizuki, I. Takano, T. Honda, and M. Sato, *Mater. Chem. Phys.* 137, 252 (2012).
7. Q. Ma, J. Hofmann, A. Litke, and E.J.M. Hensen, *Sol. Energy Mater. Sol. Cells* 141, 178 (2015).
8. L. Wang, W. Wang, Y. Chen, L. Yao, X. Zhao, H. Shi, M. Cao, Y. Liang, and A.C.S. Appl, *Mater. Interfaces* 10, 11652 (2018).
9. I.V. Bagal, N.R. Chodankar, M.A. Hassan, A. Waseem, M.A. Johar, D. Kim, and S. Ryu, *Int. J. Hydrogen Energy* 44, 21351 (2019).
10. R. Wick and S.D. Tilley, *J. Phys. Chem. C* 119, 26243 (2015).
11. L. Tsui and G. Zangari, *Electrochim. Acta* 128, 341 (2014).
12. M.M. Momeni and Y. Ghayeb, *J. Alloys Compd.* 637, 393 (2015).
13. X. Zou, G. Fang, J. Wan, X. He, H. Wang, N. Liu, H. Long, and X. Zhao, *IEEE Trans. Electron Devices* 58, 2003 (2011).
14. L. Besra and M. Liu, *Prog. Mater. Sci.* 52, 1 (2007).
15. S. Hussain, C. Cao, Z. Usman, G. Nabi, F.K. Butt, K. Mahmood, A. Ali, M. Arshad, and N. Amin, *Optik* 172, 72 (2018).
16. S. Siol, J.C. Hellmann, S.D. Tilley, M. Graetzel, J. Morasch, J. Deuermeier, W. Jaegermann, A. Klein, and A.C.S. Appl, *Mater. Interfaces* 8, 21824 (2016).
17. A. Paracchino, J.C. Brauer, J. Moser, E. Thimsen, and M. Graetzel, *J. Phys. Chem. C* 116, 7341 (2012).
18. S. Laidoudi, A.Y. Bioud, A. Azizi, G. Schmerber, J. Bartringer, S. Barre, and A. Dinia, *Semicond. Sci. Technol.* 28, 115005 (2013).
19. N.B. Mohamad-Arifin, F.B. Mohamad, N.F. Sikh-Anuar, N.B. Ahmad, N.H. Muhd-Nor, and M. Izaki, *IOP Conf. Ser.: Mater. Sci. Eng.* 226, 1 (2017).
20. S. Bijani, R. Schrebler, E.A. Dalchiele, M. Gabas, L. Martínez, and J.R. Ramos-Barrado, *J. Phys. Chem. C* 115, 21373 (2011).
21. M.A. Hossain, R. Al-Gaashani, H. Hamoudi, M.J. Al-Marri, I.A. Hussein, A. Belaidi, B.A. Merzougui, F.H. Alharbi, and N. Tabet, *Mater. Sci. Semicond. Process.* 63, 203 (2017).
22. M. Yilmaz, A.D. Handoko, I.P. Parkin, and G. Sankar, *J. Catal.* 389, 483 (2020).
23. K. Chen and D. Xue, *Mater. Focus* 1, 65 (2012).

24. P. Wang, H. Wu, Y. Tang, R. Amal, and Y. Hau Ng, *J. Phys. Chem. C* 119, 26275 (2015).
25. M. Lenglet, K. Kartouni, and D. Delahaye, *J. Appl. Electrochem.* 21, 697 (1991).
26. S. Banerjee and D. Chakravorty, *Europhys. Lett.* 52, 468 (2000).
27. R. Li, X. Yan, L. Yu, Z. Zhang, Q. Tang, and Y. Pan, *CrystEngComm* 15, 10049 (2013).
28. H. Sekhar and D.N. Rao, *J. Nanopart. Res.* 14, 976 (2012).
29. S. Chatterjee, S.K. Saha, and A.J. Pal, *Sol. Energy Mater. Sol. Cells* 147, 17 (2016).
30. L. Xiong, T. Wai Ng, Y. Yu, D. Xia, H.Y. Yip, G. Li, T. An, H. Zhao, and P. Keung Wong, *Electrochim. Acta* 153, 583 (2015).
31. Y. Tang, Z. Chen, Z. Jia, L. Zhang, and J. Li, *Mater. Lett.* 59, 434 (2005).
32. S. Shyamal, P. Hajra, H. Mandal, J.K. Singh, A.K. Satpati, S. Pande, and C. Bhattacharya, *ACS Appl. Mater. Interfaces* 7, 18344 (2015).
33. A.M. Qadir and I.Y. Erdogan, *Int. J. Hydrogen Energy* 44, 18694 (2019).